Basin Research (2008) doi: 10.1111/j.1365-2117.2008.00385.x

Distribution of Palaeozoic reworking in the Western Arunta Region and northwestern Amadeus Basin from $^{40}Ar/^{39}Ar$ thermochronology: implications for the evolution of intracratonic basins

Sandra McLaren,* Mike Sandiford,† W. James Dunlap,* Ian Scrimgeour,‡ Dorothy Close‡ and Christine Edgoose‡

*Research School of Earth Sciences, Australian National University, Acton, Australian Capital Territory, Australia
†School of Earth Sciences, University of Melbourne, Victoria, Australia
‡Northern Territory Geological Survey, Darwin, Northern Territory, Australia

ABSTRACT

The Centralian Superbasin in central Australia is one of the most extensive intracratonic basins known from a stable continental setting, but the factors controlling its formation and subsequent structural dismemberment continue to be debated. Argon thermochronology of K-feldspar, sensitive to a broad range of temperatures (~150 to 350 °C), provides evidence for the former extent and thickness of the superbasin and points toward thickening of the superbasin succession over the now exhumed Arunta Region basement. These data suggest that before Palaeozoic tectonism, there was around 5–6 km of sediment present over what is now the northern margin of the Amadeus Basin, and, if the Centralian superbasin was continuous, between 6 and 8 km over the now exhumed basement. $^{40}Ar/^{39}Ar$ data from neoformed fine-grained muscovite suggests that Palaeozoic deformation and new mineral growth occurred during the earliest compressional phase of the Alice Springs Orogeny (ASO) (440–375 Ma) and was restricted to shear zones. Significantly, several shear zones active during the late Mesoproterozoic Teapot Orogeny were not reactivated at this time, suggesting that the presence of pre-existing structures was not the only controlling factor in localizing Palaeozoic deformation. A range of Palaeozoic ages of 440–300 Ma from samples within and external to shear zones points to thermal disturbance from at least the early Silurian through until the late Carboniferous and suggests final cooling and exhumation of the terrane in this interval. The absence of evidence for active deformation and/or new mineral growth in the late stages of the ASO (350–300 Ma) is consistent with a change in orogenic dynamics from thick-skinned regionally extensive deformation to a more restricted localized high-geothermal gradient event.

INTRODUCTION

Intracratonic basins form major sediment stores on all continental masses. Despite their economic and environmental importance, the factors that control their formation and subsequent evolution are only poorly understood. In Australia, major intracratonic basins are known from the Late Neoproterozoic to Early Palaeozoic, as well as the Mesozoic (e.g., the Eromanga Basin). The older Late Neoproterozoic to Early Palaeozoic basins include the Amadeus, Georgina, Ngalia and eastern Officer Basins (Fig. 1). It is generally accepted that these basins form a series of partly linked and partly structurally dismembered remnants of a formerly more extensive basin known as the Centralian Superbasin (e.g., Walter *et al.*, 1995; Haines *et al.*, 2001). The former extent of the Superbasin, and the processes responsible for its structural dismemberment, are the subject of ongoing debate. As the Centralian Superbasin is one of the most extensive and well-documented intracratonic basins in the world, these issues are highly relevant to more general questions of the origin and evolution of intracratonic basins.

The structural dismemberment of the Centralian Superbasin is evident in thrust and fold-nappe complexes along present day basin margins. Structural vergence criteria imply significant exhumation of the underlying crust in basement blocks, such as the Arunta and Musgrave Regions (Fig. 1) that now separate individual basins. The intensity of the intraplate tectonism is evident in the extraordinary gravity anomalies of central Australia, which

Correspondence: Sandra McLaren, School of Earth Sciences, University of Melbourne, Victoria 3010, Australia. E-mail: mclarens@unimelb.edu.au

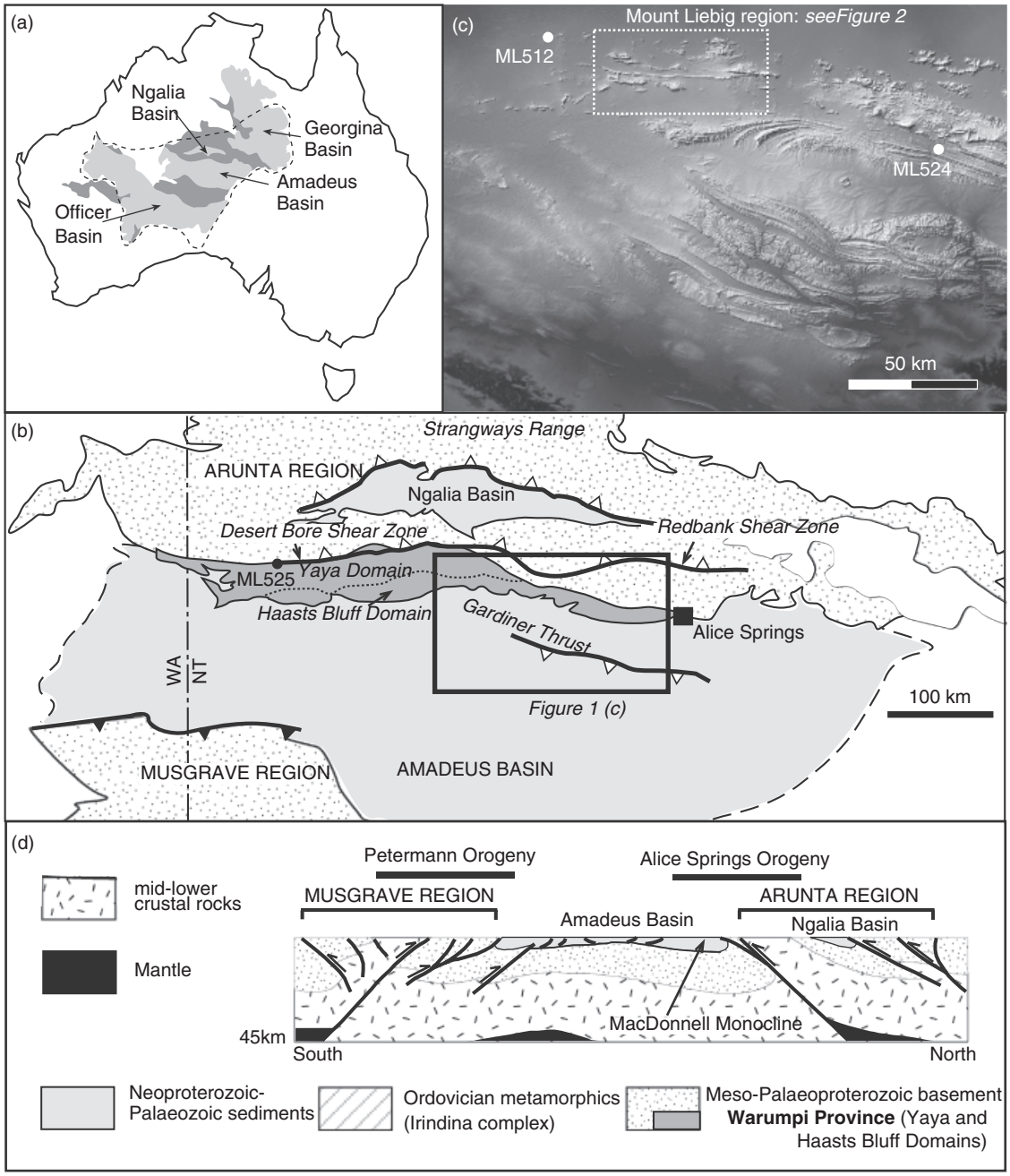

Fig. 1. (a) Dashed line indicates the former extent of the intracratonic Centralian Superbasin, recording sedimentation in the interval from the Neoproterozoic to the Devonian. Remnants of the Centralian Superbasin, the Officer, Ngalia, Amadeus and Georgina Basins are shown in light shading together with now exhumed Palaeo–Mesoproterozic basement blocks (indicated in dark shading). (b) Regional geological framework of the Arunta Region and Amadeus Basin; location of sample ML525 from Mount Rennie shown. The Desert Bore Shear Zone in the Mount Liebig region and the Redbank Shear Zone near Alice Springs together form part of the Central Australian Suture (Scrimgeour *et al.*, 2005a). (c) Digital elevation model of central Australia showing the prominent strike-ridges of the Amadeus Basin sediments as a result of Palaeozoic basin-inversion. Location of Mount Liebig region is indicated by dashed line. (d) Schematic cross-section showing basin geometry and location of major intraplate orogenic events; modified from Sandiford & Hand (1998).

are amongst the largest known from the continental interiors (Mathur, 1976). An intriguing aspect of the structural dismemberment in central Australia is that it occurred in a series of spatially and temporally distinct intraplate orogenies, known as the Alice Springs and Petermann Ranges Orogenies (e.g., Collins & Teyssier, 1989; Shaw *et al.*, 1992; Dunlap & Teyssier, 1995; Camacho *et al.*, 1997; Sandiford & Hand, 1998).

In a series of contributions Sandiford & Hand (1998), Hand & Sandiford (1999) and Sandiford (2002), have suggested a link between the development of the Centralian Superbasin and its subsequent structural dismember-

ment. They suggested that the locus of deformation mirrored changes in thickness of basin successions inferred by interpolating isopach data. Camacho *et al.* (2002) challenged this notion by arguing that detrital zircon provenance and thermochronological data precluded significant burial of the Musgrave Region during the Neoproterozoic. While Camacho *et al.* (2002) concurred with the earlier work in suggesting deformation was driven by far-field stresses originating from plate boundaries, they suggested that the primary reason for localisation was the existence of inherited structures. In our view, this somewhat conventional interpretation fails to explain some important and enigmatic aspects of the Centralian basins, including:

(1) why the locus of intraplate deformation has moved around in space and time, rather than having been localized in one place (see discussion by Hand & Sandiford, 1999), and
(2) why the major 'inversion' structures verge basinward, an orientation inconsistent with reactivation of any plausible geometry of basin forming normal faults (e.g., Sandiford *et al.*, 2001)

In this paper, we adopt a different approach to understanding the evolution of the Centralian Superbasin in the region of the western Arunta Region, using K-feldspar $^{40}Ar/^{39}Ar$ thermochronological data (Lovera *et al.*, 1989). K-feldspars are sensitive to argon loss over a broad range of temperatures ($\sim$150 to 350 °C) appropriate to the range of thermal regimes that were likely to have operated at the base of the Centralian Superbasin before subsequent inversion. For example, the MacDonnell Monocline, along the northern margin of the Amadeus Basin, exposes a $\sim$5 to 7 km thick succession of Neoproterozoic-Palaeozoic sediment. Modern-day temperature gradients of up to $\sim$30 to 35 °C km^{-1} (Gorter, 1984) imply temperatures in the range of $\sim$150 to 250 °C at the basal unconformity before exhumation. Although the K-feldspar multiple-diffusion-domain (MDD) approach has been the subject of debate (e.g., Parsons *et al.*, 1999), we have previously shown that it is capable of providing unique, regionally consistent, insights into the evolution of intracratonic basins (McLaren *et al.*, 2002; McLaren & Dunlap, 2006). Here, we present the results of K-feldspar MDD modelling, in combination with conventional $^{40}Ar/^{39}Ar$ mica thermometry, from a number of samples from the northwestern Amadeus Basin and the adjacent parts of the western Arunta Region (Fig. 1).

These analyses, together with previously published work, shed light on the former distribution of the Centralian Superbasin, and the processes responsible for its formation and subsequent inversion. We begin by outlining the regional geological framework of the analysed samples, followed by presentation and interpretation of the thermochronological data.

REGIONAL SETTING

Samples were obtained for this study from a wide area of the western Arunta Region. Most samples are from the Mount Liebig region (Figs 1 and 2), but we also sampled material from Ellery Creek to the east, and the Mount Rennie region further to the west (Fig. 1). The area of study consists of both the late Palaeoproterozoic Warumpi Province of the Arunta Region (local 'basement') and the Neoproterozoic to Palaeozoic Amadeus Basin (local 'cover'). In the Mount Liebig region, these units are interleaved along a series of major shear zones.

Warumpi province

The Warumpi Province forms part of the Arunta Region in central Australia (Fig. 1). The Arunta Region records a complex Palaeo-Mesoproterozoic history and, together with the overlying Neoproterozoic-Palaeozoic cover, has suffered extensive Palaeozoic reactivation. The Warumpi Province in the Mount Liebig area consists of two fault-bounded domains: the largely amphibolite facies Haasts Bluff Domain in the south, and the dominantly granulite facies Yaya Domain in the north. These regions have distinct protolith ages (Scrimgeour *et al.*, 2005a) and record three major Proterozoic tectonothermal events: the Liebig Orogeny (1640–1635 Ma; Scrimgeour *et al.*, 2005b); the Chewings Orogeny (1590–1570 Ma; Teyssier *et al.*, 1988) and the Teapot Event (*c.* 1150 Ma; Shaw *et al.*, 1992).

Evidence for the Liebig Orogeny is found in rare relict low-strain zones throughout the Mount Liebig region. Metamorphism was medium-pressure granulite facies in the Yaya Domain, and upper amphibolite facies in the Haasts Bluff Domain. High-grade assemblages include orthopyroxene-sillimanite-garnet granulites and silica-undersaturated sapphirine-, corundum- and kornerupine-bearing lithologies. The highest grade orthopyroxene+sillimanite assemblages in the Yaya Domain imply temperatures of $\sim$900 °C and pressures of $>$8 kbar (Scrimgeour *et al.*, 2005a). Peak conditions in the Haasts Bluff Domain range between 700–750 °C and 8.5–9 kbar (Scrimgeour *et al.*, 2005a). The timing of the Liebig Orogeny is constrained by SHRIMP U-Pb dating of metamorphic zircon rims from the Inyalinga Granulite giving ages of 1638 $\pm$ 8 and 1636 $\pm$ 6 Ma (Scrimgeour *et al.*, 2005b).

The Chewings Orogeny resulted in pervasive overprinting of Liebig Orogeny structures throughout the Mount Liebig area. This orogeny was a major event that affected the entire Warumpi Province in the interval 1590–1570 Ma. Kinematic indicators in the Mount Liebig region suggest a north over south sense of movement. Assemblages in the Yaya Domain record peak temperatures and pressures of 680–700 °C and 5.5–6.5 kbar, respectively; assemblages in the Haasts Bluff Domain record temperatures of 490–630 °C and 4.5–6 kbar (Scrimgeour *et al.*, 2005a). The timing of the Chewings Orogeny is constrained by SHRIMP U-Pb ages of 1590 $\pm$ 4 and

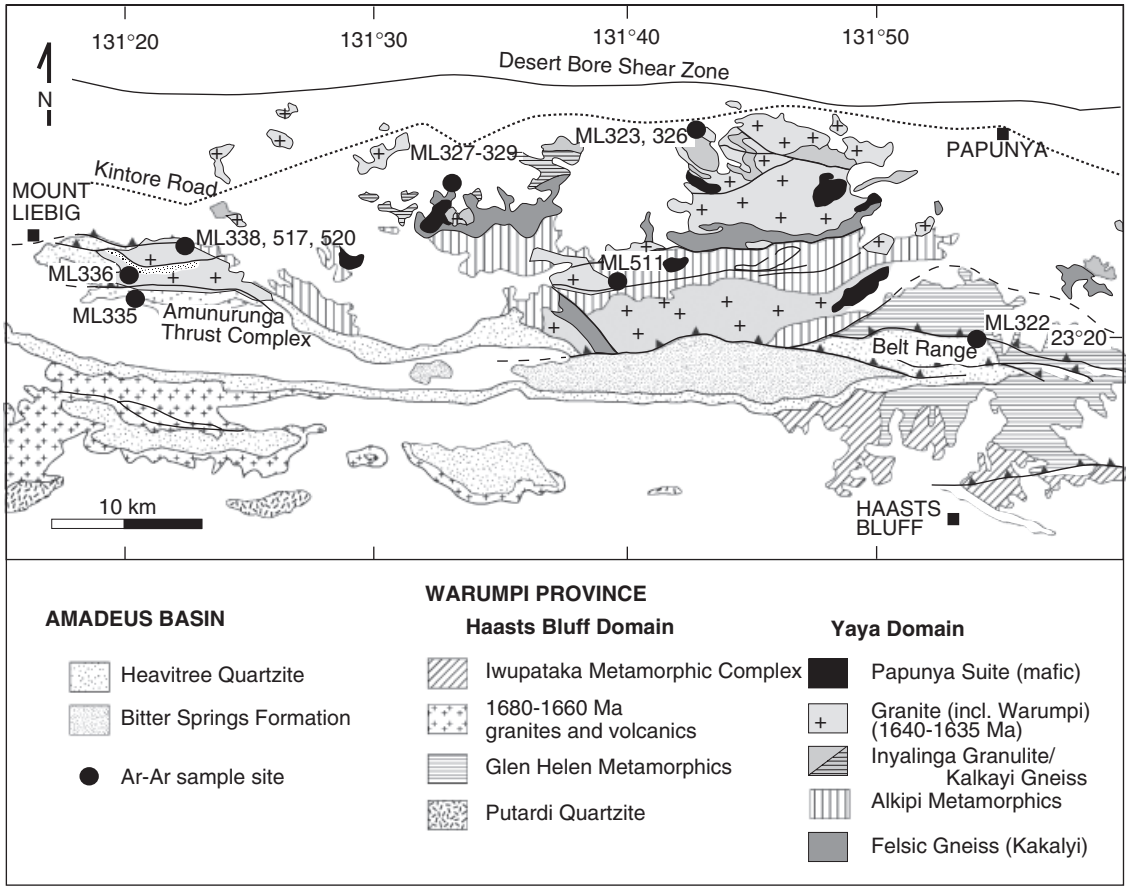

Fig. 2. Mount Liebig region – simplified geological map including sample locations.

1585 ± 8 Ma from high-U rims on zircons within the Warumpi Granite (Page, 1996), and of 1571 ± 5 Ma from metamorphic zircon rims in the Kakalyi Gneiss (Kinny, 2002).

The Teapot Event is the last major Proterozoic event recorded in the Mount Liebig region. It is a predominantly thermal event recorded between 1150 and 1130 Ma that may have been related to magmatism and metamorphism in the Musgrave Region (Edgoose *et al.*, 2004). Regional resetting of hornblende $^{40}Ar/^{39}Ar$ isotopic systems throughout the Warumpi Province (Shaw *et al.*, 1992; Biermeier *et al.*, 2003) implies regional temperatures higher than 500 °C. In the Mount Liebig area metamorphic grade was higher, locally reaching upper amphibolite facies (> 650 °C) in the Kakalyi Gneiss where locally intense migmatization is observed. Metamorphic zircon rims of 1149 ± 3 Ma in the Kakalyi Gneiss, and isotopic disturbance of zircons from other lithologies constrain the timing of this event (Scrimgeour *et al.*, 2005a).

Amadeus Basin

The Amadeus Basin is a large early Neoproterozoic to Devonian east–west trending intracratonic basin forming part of the extensive Centralian Superbasin (e.g., Walter *et al.*, 1995; Haines *et al.*, 2001). The basin uncomformably overlies the Warumpi Province throughout central Australia.

The Heavitree Quartzite is the basal unit of the basin and forms many prominent strike ridges throughout the Mount Liebig and western MacDonnell regions (Figs 1 and 2). It is dominated by silicified quartz-sandstone and is of variable thickness. Age of deposition is thought to be between 1050 and 800 Ma, constrained by the age of the underlying Kulgera dyke swarm in the southern Arunta Region, the youngest detrital zircon ages of *c.* 1100 Ma (Maidment *et al.*, 2007) and an age of *c.* 790–800 Ma (Zhao *et al.*, 1992) for the conformably overlying Bitter Springs Formation, a succession of carbonates, evaporites and fine-grained clastic sediments.

Unconformably overlying the Bitter Springs Formation is the Areyonga Formation, a diamictite conglomerate, calcareous and lithic sandstone related to the Sturtian glaciation (Wells, 1981). As this unit does not crop out in the Mount Liebig region, it was sampled for this study from Ellery Creek (Sample ML524 indicated on Fig. 1). The conglomerate material is extremely poorly sorted and contains abundant basement-derived clasts as well as clasts of both Heavitree Quartzite and Bitter Springs Formation.

Following deposition of the Heavitree Quartzite and Bitter Springs Formation, subsidence and sediment accumulation in the Centralian Superbasin continued episodically, interrupted by a series of Palaeozoic orogenic events (Fig. 3). Shaw (1991) identified nine tectonostratigraphic packages in the interval 900–360 Ma, corresponding to

changes in sea-level, changes in basin morphology and variations in sediment supply, and related at least in part to the uplift of basin and basement blocks during episodic orogenesis.

Palaeozoic intraplate orogenic events

The Petermann Ranges Orogeny, in the latest Neoproterozoic to early Cambrian (570–530 Ma), was the first Palaeozoic intraplate orogenic event to affect central Australia. It resulted in uplift and exposure of the Palaeo-Mesoproterozoic basement of the Musgrave Region and deformation and exhumation of the southwestern Amadeus Basin (Camacho *et al*., 1997; Scrimgeour & Close, 1999), together with deposition of syn-orogenic sediments of the Arumbera Sandstone in the Amadeus Basin.

Sedimentation continued in the basin in the Early Palaeozoic, extending south to the Officer Basin, north to the Georgina and Wiso Basins, east to the Warburton Basin and west to the Canning Basin (Haines *et al*., 2001). An extensional high-grade early Ordovician metamorphic episode in the Arunta region, the Larapinta Event, appears to be coeval with this period of sedimentation, correlating with deposition of thick marine sequences of the Larapinta Group in the northern Amadeus Basin (Hand *et al*., 1999; Mawby *et al*., 1999).

The last major period of intraplate tectonism occurred during the Alice Springs Orogeny (ASO). The ASO was a term introduced by Forman (1966) for the deformational event affecting the late Devonian Pertnjara Group. Definition of the orogeny was subsequently extended by Bradshaw & Evans (1988) to include all convergent deformation in central Australia from the Rodingan Movement (around 440–450 Ma), which resulted in the exhumation of the eastern Arunta Region and erosion of the northeastern Amadeus Basin, to the late Permian Waite Creek Movement. More recently (e.g., Shaw, 1991) the ASO has been used to describe only that deformation in the interval between 400 and 300 Ma, beginning with the Pertnjara Movement. However, definition of the event is a topic of ongoing debate and many authors continue to attribute the Rodingan Event to the long-lived ASO. It is commonly agreed that the ASO ceased around 325 Ma, the youngest ages recorded by various isotopic systems.

In the Mount Liebig Region, Scrimgeour *et al*. (2005a) suggest that tectonism and exhumation is likely to have commenced during the Rodingan Event, with erosion leading to increased clastic input into the western and southern Amadeus Basin. A period of tectonic quiescence in the Silurian led to the deposition of the regionally extensive Mereenie Sandstone. This was followed by significant south-directed compressional deformation and crustal shortening, attributed to the main (400–380 Ma) phase of the ASO (Scrimgeour *et al*., 2005a). Most ASO structures within the Arunta Region dip moderately to steeply to the north and have stretching lineations that plunge north–northeast.

In the Mount Liebig region low-grade shear zones apparently related to the ASO interleave Warumpi Province rocks with basal units of the Amadeus Basin. This structural interleaving is confined to the Heavitree Quartzite and Bitter Springs Formation, suggesting a major decollement within the Bitter Springs Formation (e.g., Marjoribanks, 1976; Teyssier, 1985; Korsch & Lindsay, 1989; Flöttmann & Hand, 1999). The major structural features in the Mount Liebig region include the Edward and Stokes Thrust Complexes in the Belt Range; the Amunurunga Thrust Complex in the vicinity of the Mount Liebig community; and the Desert Bore Shear Zone in the north of the area (Fig. 2). The Edward and Stokes, and Amunurunga complexes comprise north-dipping, south-directed thrusts that juxtapose basement over Heavitree Quartzite. The Desert Bore Shear Zone is a large-scale east–west trending structure that extends west from Mount Liebig to near the Western Australian border (Figs 1 and 2). The Desert Bore Shear Zone forms part of the Central Australian Suture (Scrimgeour *et al*., 2005a), a newly defined term describing the structural boundary between the Warumpi and Aileron Provinces; to the east of Mount Liebig the Central Australian Suture includes the Redbank Shear Zone (Fig. 1). The intensity of deformation and apparent degree of shortening decrease to the west across the Mount Liebig area. The metamorphic grade in the Belt Range and Amunurunga Range is middle to lower greenschist facies with fine-grained muscovite growth and ribbon deformation of quartz (e.g., Dunlap *et al*., 1997). The metamorphic grade north of the ranges is less well constrained due to poor exposure but some mylonites may have locally reached upper greenschist facies conditions (Scrimgeour *et al*., 2005a).

$^{40}Ar/^{39}Ar$ ANALYSIS

At very high temperatures all the radiogenic argon ($^{40}Ar^{*}$) produced by decay of ^{40}K is expected to be lost continuously from a crystal lattice by volume diffusion. As a mineral cools it will reach a temperature below which argon diffusion is negligible, so that the argon daughter product accumulates quantitatively. A K/Ar age or a $^{40}Ar/^{39}Ar$ total fusion age essentially records the time since closure of the mineral to argon diffusion. In general, for cooling rates typical of orogenesis (Dunlap, 2000), the temperature interval over which a mineral passes from little accumulation to full retention of radiogenic argon is restricted (e.g., a few tens of degrees). Common potassium-bearing minerals have a large range of closure temperatures with respect to argon accumulation. Hornblende has a T_c of $\sim$500 °C (Harrison, 1981); muscovite has an estimated T_c of $\sim$400 °C (Hames & Bowring, 1994), biotite a T_c of $\sim$300 °C (Harrison *et al*., 1985) and K-feldspar appears to exhibit a range of closure temperatures from about 350 °C to 150 °C (Lovera *et al*., 1989). Analysis of a number of different minerals from a particular region by the K/Ar

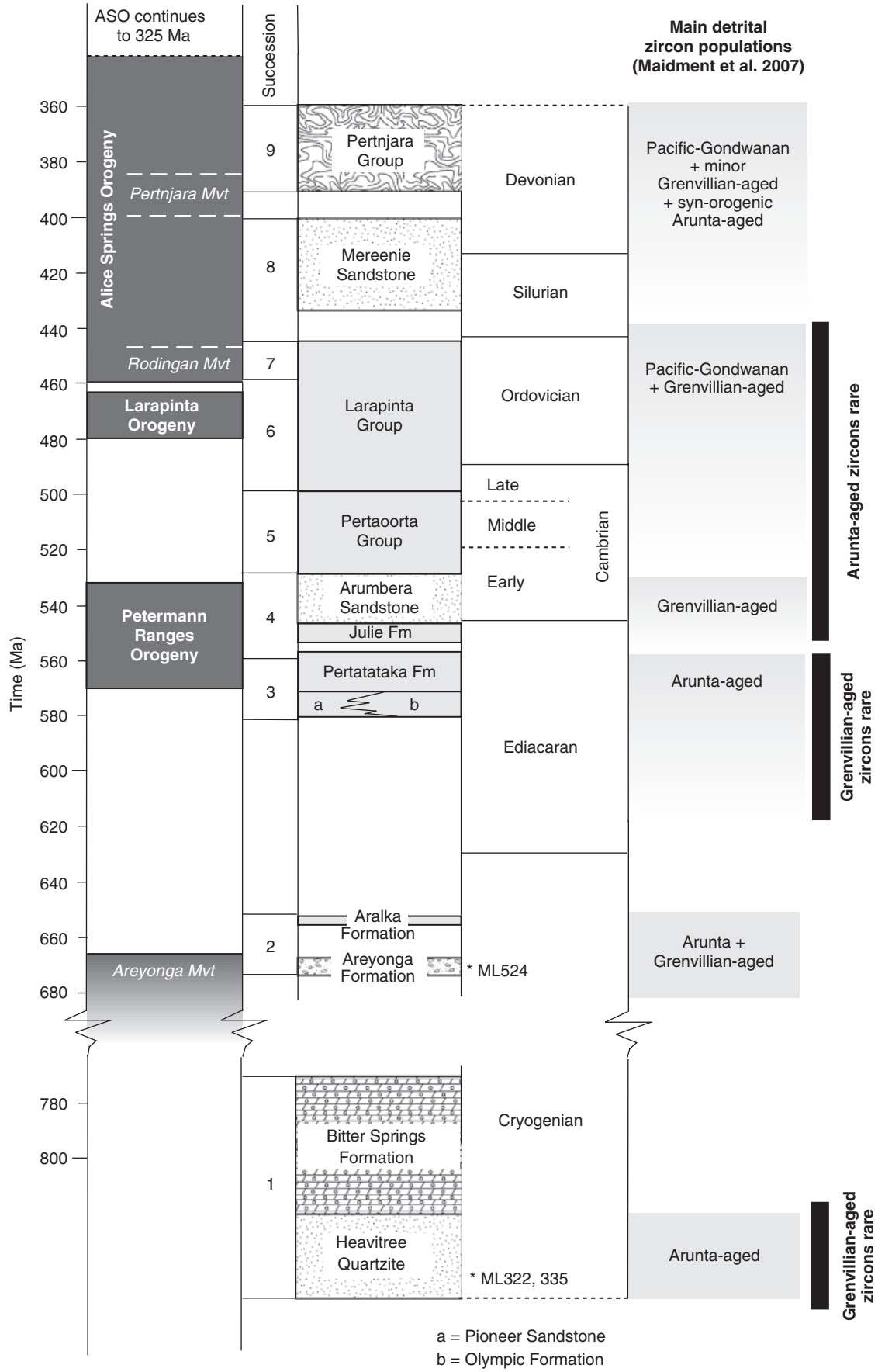

and $^{40}Ar/^{39}Ar$ techniques allows a cooling history to be elucidated.

Slow cooling of a mineral can result in the development of radiogenic argon concentration gradients, especially adjacent to inter- or intragrain boundaries. Step heating of a sample that has been irradiated in a nuclear reactor to produce ^{39}Ar from ^{39}K (see McDougall & Harrison, 1999), may reveal variations in the $^{40}Ar^*/^{39}Ar_K$ ratio (which is proportional to age) if the mineral remains stable during at least part of the heating experiment. Results generally are shown as an age spectrum, a plot of age of each step against the cumulative proportion of ^{39}Ar released. Early workers proposed criteria for the identification of a plateau in an age spectrum (see McDougall & Harrison, 1999, for discussion). Here, the term plateau is used only for that part of an age spectrum where the ages of consecutive steps are within 2σ of one another and together comprise at least 50% of the gas release. We also use the term 'plateau-like' for a series of steps within an age spectrum that do not meet these criteria, mainly due to the presence of one or two discordant steps within a sequence of steps otherwise within 2σ of one another. The location of samples analysed is shown in Figs 1 and 2.

Hornblendes

Two hornblende mineral separates were analysed using the $^{40}Ar/^{39}Ar$ technique. Sample ML326 is the most northerly of the pair, and is from a mafic amphibolite adjacent to a shear zone in the northern central zone of the Mount Liebig region. The age spectrum of hornblende from this sample is strongly contaminated by excess argon for around the first 20% of the gas release (Fig. 4). Ages in the non-contaminated portion of the spectrum range from ~1250 to ~1840 Ma. No plateau or plateau-like segment is achieved. The total-gas age is 2079 ± 7 Ma.

Sample ML328 is an amphibolite from the Inyalinga Granulite near Yaya Creek, slightly south of Sample ML326. Hornblende from this sample yields a slightly disturbed age spectrum with a total gas age of 1162 ± 4 Ma. The youngest ages are around 760 Ma but >90% of the gas is the age range 1150–1200 Ma (Fig. 4).

Micas

Nine muscovite and three biotite mineral separates were analysed and reveal a wide spread of apparent ages (Figs 4 and 5). Three of the muscovite mineral separates (ML322, ML323 and ML335) could only be prepared using heavy liquid centrifuge techniques as they are moderately fine grained (<75 μm). All other separates were obtained using conventional methods (Appendix A).

Muscovite ML525, from a mylonite zone in the Mount Rennie region (Fig. 1), shows a disturbed age spectrum that ranges in age from ~810 to ~1000 Ma, with a total gas age of 916 ± 2 Ma. The slight hump-shape may be indicative of excess argon in the early released gas, or the presence of some contaminating phase. No plateau or plateau-like age is achieved.

Muscovite ML338 from quartzite of the Alkipi Metamorphics in the north-western Mount Liebig range records ages between 900 and 1100 Ma, with >80% of the gas older than 1050 Ma. The total-gas age is 1056 ± 6 Ma. Muscovite ML517 from the nearby Inyalinga Granulite exhibits an age spectrum very similar in shape and age to that of ML525. In the first 55% of the gas released ages range from 640–1000 Ma; the remaining gas exhibits ages from 960–1100 Ma. Here, the hump-shape is quite pronounced. The total gas age is 969 ± 3 Ma; no plateau or plateau-like age is achieved.

Muscovite ML511, from the Alkipi Metamorphics of the central Mount Liebig range, records younger ages between 600 and 950 Ma, with a total-gas age of 834 ± 5 Ma. This age spectrum exhibits classic staircase geometry, and no plateau or plateau-like segment is achieved. Co-lithic biotite ML511 shows a similar, but older, range of ages to that of muscovite ML511. The ages in the spectrum range from 640 Ma in the first step to 990 Ma in the last step. The total-gas age of this sample is 955 ± 4 Ma. Given that the two samples are of approximately the same grain-size range (125–250 μm), this age relationship is unexpected as the established closure temperature range of biotite is lower than that of muscovite. Both age spectra are monotonically increasing and show none of the typical features of excess argon related contamination. From the data presented here, we know that new muscovite was growing in the Liebig Region during the ASO, but that new biotite was not. Scaillet *et al.* (1992) and Hames & Cheney (1997) have shown that argon diffusivity in muscovite may be significantly lower than previously suggested, and that pre-existing muscovite may suffer partial loss of accumulated $^{40}Ar^*$ due to chemical alteration or recrystallization, particularly during long crustal residence times. This may have occurred in the Mount Liebig Region during slow Palaeozoic reheating and may explain the differences in apparent age between co-lithic muscovite and biotite in Sample ML511. The difference may also be attributed to abnormally retentive biotite (as seen in some high grade biotites) or differences in diffusivity related to differences in biotite composition (e.g., Dahl, 1996; Lo *et al.*, 2000).

Muscovite ML322 from the Heavitree Quartzite, the most southerly sample analysed from the eastern Mount Liebig range, also exhibits a slightly disturbed age spec-

Fig. 3. Stratigraphic and tectonic framework of the Amadeus Basin, central Australia. Numbers 1–9 refer to the sedimentary successions defined by Shaw (1991). Stratigraphic position of samples ML322, ML335 and ML524 is indicated. Also shown is a summary of the detrital zircon data of Maidment *et al.* (2007) showing changing patterns of zircon provenance. Pertatataka Formation includes the Cyclops Member (Lindsay & Korsch, 1991). Age of the Petermann Ranges Orogeny from Camacho *et al.* (1997).

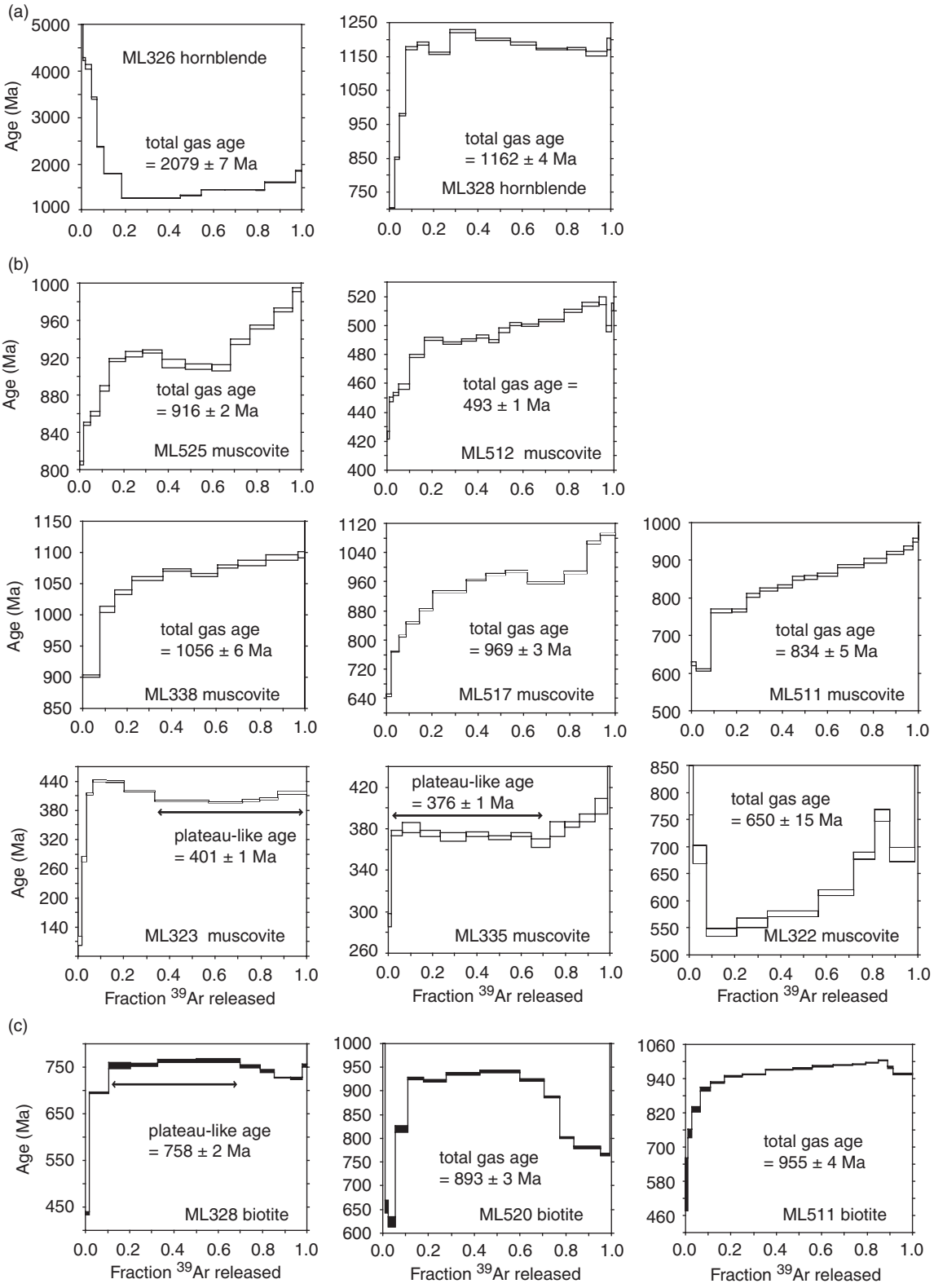

Fig. 4. $^{40}Ar/^{39}Ar$ age spectra for hornblende, muscovite and biotite samples. Note that vertical scales are different in each figure in order to maximize the clarity of each individual age spectrum. Age spectra are shown in approximate relative position, West to East and North to South; see maps shown in Figs 1 and 2.

trum with evidence for excess argon in the first 10% of the gas release. The remaining 90% of the gas exhibits ages rising from 540 to 700 Ma. No plateau or plateau-like segment is achieved. The total-gas age is 650 ± 15 Ma.

Biotite ML328, from the Inyalinga Granulite near Yaya Creek, exhibits a range of ages from 440 to ~760 Ma, however, only the first 2–3% of the gas released is younger than 680 Ma. The sample has a plateau-like segment of

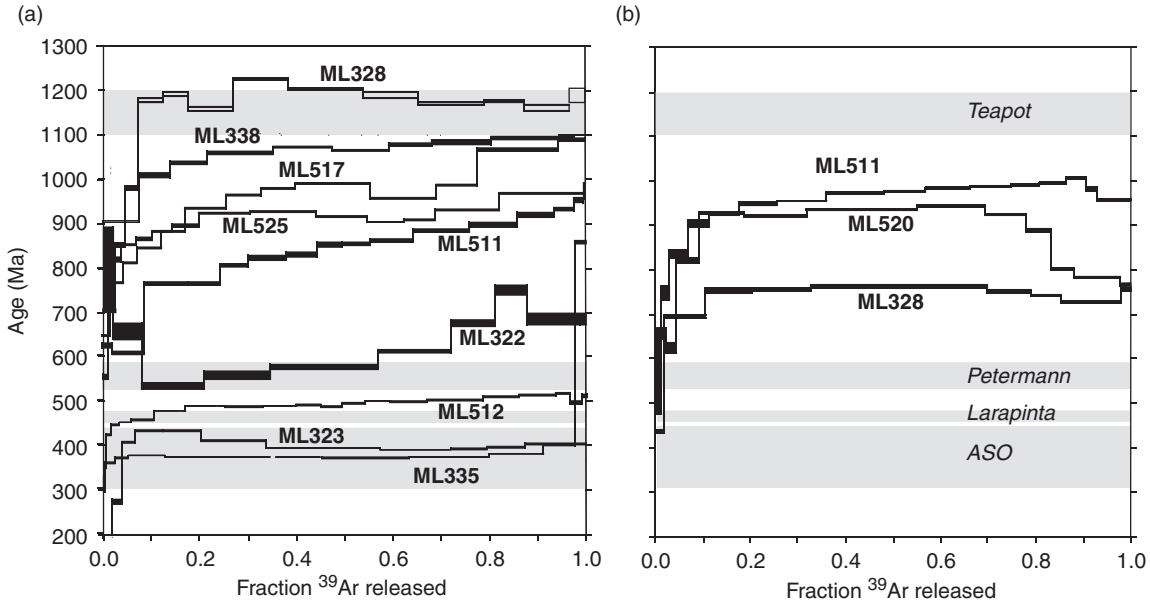

Fig. 5. Summary of $^{40}Ar/^{39}Ar$ age spectra for all samples: (a) hornblende (open symbols) and muscovite (closed symbols); (b) biotite. Major events including the Teapot, Petermann Ranges and Alice Springs Orogenies are indicated.

758 ± 2 Ma and a total-gas age of 743 ± 3 Ma. Biotite ML520 from a felsic gneiss of the Yaya Domain also exhibits a wide range of ages and is characterized by a disturbed convex-upward age spectrum. Ages range from 625 to 1050 Ma. It has a total gas age of 893 ± 3 Ma and no plateau or plateau-like age is achieved.

In contrast to the dominantly Neoproterozoic ages recorded by these samples, muscovite ML512 and the <75 μm muscovite separates from samples ML335 and ML323 record Palaeozoic ages younger than ~520 Ma. Sample ML512, a muscovite-bearing splay of the Desert Bore Shear zone north-west of the Mount Liebig community (Fig. 1), yields ages between 420 and 520 Ma. Around 90% of the gas released is older than 480 Ma and the total-gas age is 493 ± 1 Ma. Sample ML335, strained Heavitree Quartzite from the southern Mount Liebig range, yields comparatively young ages, with over 80% of the gas < 400 Ma. For this sample a plateau-like segment of 376 ± 1 Ma and the total-gas age of 390 ± 1 Ma are closely matched. Sample ML323 is a garnet–muscovite–chlorite schist from a mylonite zone in the northern Mount Liebig range and it also records Ordovician to Devonian ages. It is characterized by ages as young as 100 Ma in the earliest released gas, and also by a slight hump-shaped spectrum between 5 and 30% of the gas release. A plateau-like segment of 401 ± 1 Ma is achieved for the 30–70% portion of the age spectrum. This plateau-like segment closely matches the total-gas age of 403 ± 2 Ma.

K-feldspars

Six K-feldspar samples were analysed by the $^{40}Ar/^{39}Ar$ method. Only three of the samples (ML524, ML336 and ML520) exhibit age spectra characterized by ages that increase, essentially monotonically, as temperature is raised. The remaining samples (ML329, ML327 and ML511) all display highly disturbed age spectra that alternate between old and young ages at each isothermal step (Fig. 6). Unlike common chlorine-related excess argon patterns, where contamination is generally only seen in the first 5–10% of the gas release, the Mount Liebig samples display this pattern for the first 50–70% of the gas release (Fig. 6). However, despite the unusual age spectra that characterize

Fig. 6. Tectonic sketch map of Mount Liebig region and summary of $^{40}Ar/^{39}Ar$ age spectra for K-feldspar samples, showing measured and modelled age spectra and preferred thermal histories. The upper figure of each pair shows the calculated age against the fraction of ^{39}Ar released for laboratory and model results. Laboratory results (including 1σ errors in the measured ages) are shown by solid lines. Modelled spectra are shown by dashed lines. Note that vertical scales are different in each figure in order to maximize the clarity of each individual age spectrum. The lower figure of each pair shows the temperature–time plot of the preferred thermal history used to generate the best- fit model. The shaded region shows the range of variation about this average history, which mainly illustrates the effect of the uncertainty in estimates of activation energy. For Sample ML520 the dashed line represents the preferred fit to the laboratory age spectrum obtained using the manual iterative method. For Sample ML524 the dashed lines represent the range of thermal histories that provide equally good fits to the laboratory age spectrum, showing that the modelled age spectrum is insensitive to Sturtian ages of Areyonga Formation in the range 720–660 Ma (Lindsay, 1989; Corsetti *et al.*, 2006). Diffusion coefficient, relative volume fraction and relative domain size for each sample are given in Table 2.

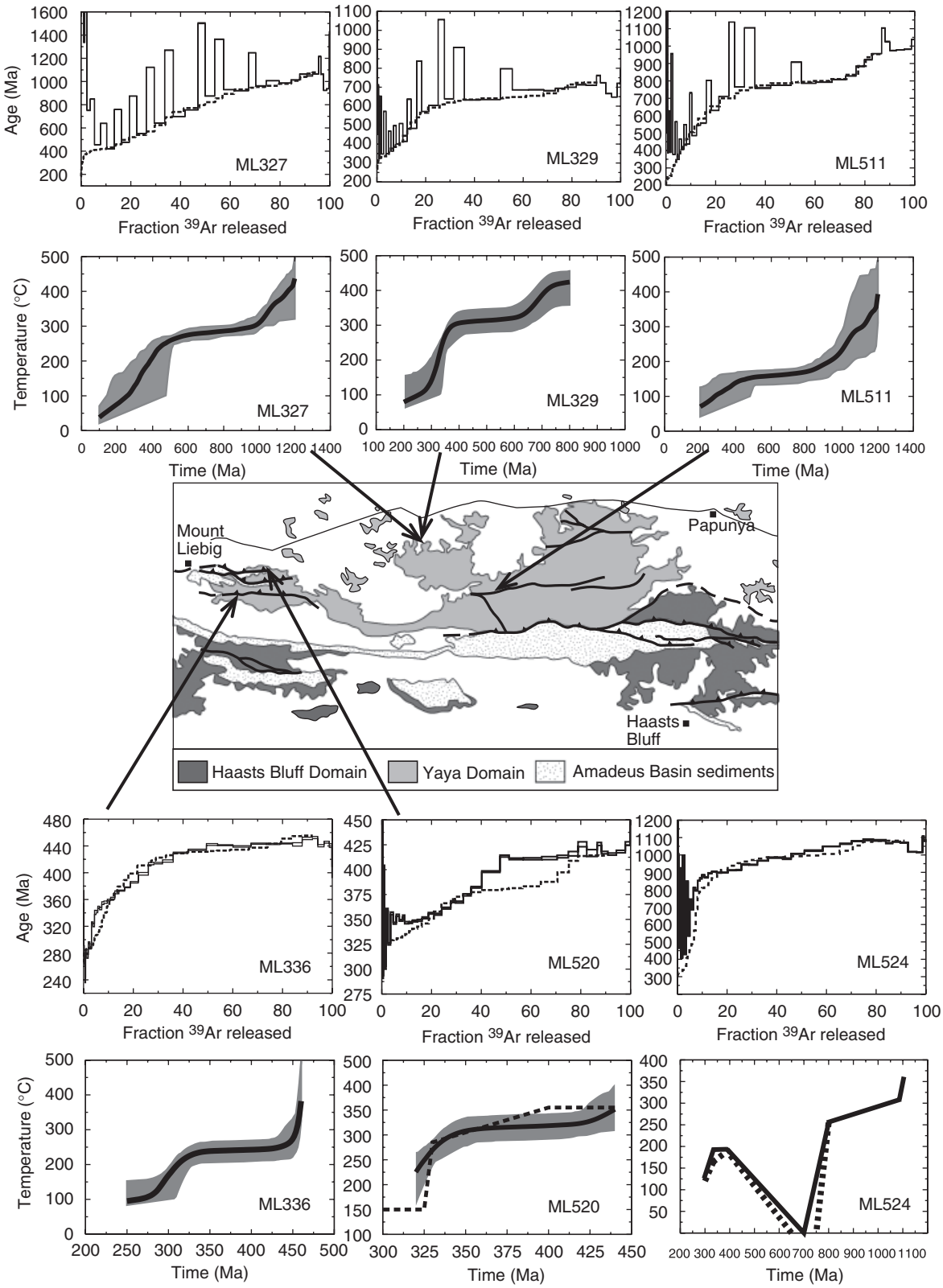

these samples, some useful observations can be made and these are discussed below.

For all K-feldspar samples, regardless of location or stratigraphic position, the youngest ages recorded are in the range 280–400 Ma indicating significant argon loss during the mid to late Palaeozoic. The oldest ages range from 430 Ma for sample ML336 to 1150 Ma for sample ML327, suggesting that in some areas temperatures did not exceed 350 °C for extended periods following the Teapot Orogenic event.

K-feldspar ML524 is from a boulder clast within the glacial Areyonga Formation at Ellery Creek. Its age spectrum is contaminated by excess argon for the first 10% of the gas release, but then exhibits a remarkably smooth increase in age from ~850 to 1100 Ma.

This pattern of increasing age is also noted in sample ML336, from a gneissic granite in the southern Mount Liebig range. The age spectrum of this sample increases from ~280 to 450 Ma. There is very minor excess argon in the first 2–3% of the gas release. A plateau-like segment with an age of *c*. 440 Ma is achieved over the 50–85% portion of the gas released.

K-feldspar ML520, also from a felsic basement gneiss, exhibits a range of ages from 300 to 430 Ma. It is characterized by a strong age gradient for the first 50% of the gas release, and a plateau-like segment of ~420 Ma for the remaining gas release. It is contaminated by excess argon for the first 10% of the gas release. Thereafter the gas increases in age from 346 to 416 Ma.

As noted above, K-feldspars ML511, ML327 and ML329 all show disturbed age spectra (Fig. 6). These unusual patterns are possibly due to the presence of two populations of fluid inclusions, each with different retentivities for ^{40}Ar, or alternatively, to the breakdown of a contaminating phase with high ^{40}Ar retentivity which is not discernible through examination of the mineral separate or the thin section. We note, however, that the isothermal steps in the heating schedule to which each sample was subject represent best practice in identifying samples that may show this behaviour. If each first, older age, step in each isothermal heating series is discarded, in the same way as advocated for early released chlorine derived excess argon, the remaining minima-ages can be used to better define the cooling envelope. Here, all three contaminated samples record Proterozoic ages, with maxima ~750 Ma for K-feldspar ML329, and ~1100 Ma for K-feldspars ML511 and ML327. As will be discussed below, these maximum ages are within a range that is not unreasonable given similar observations from basement gneisses across the Arunta that have experienced only mild tectonism in the Palaeozoic. We note that K-feldspar ML329 was sampled from a shear zone (Table 1) and its younger range of ages is interpreted to reflect reactivation of this structure (see 'Reheating histories').

MDD ANALYSIS OF K-FELDSPARS

We have interpreted the K-feldspar age spectra using the MDD method described by Lovera *et al*. (1989) and Richter *et al*. (1991) and the software available from *http://sims.ess.ucla.edu/argonlab/programs.html*. This method assumes that the release of argon is by a thermally activated volume diffusion process described by the Arrhenius equation. Calculated Arrhenius relationships for K-feldspars are commonly convex upward, showing a significant deviation from linearity, consistent with diffusion occurring over a range of length scales (Lovera *et al*., 1989). For each Arrhenius plot, the slope of the linear array of points

Table 1. Sample location and Description

Sample	hbde	mu	bt	Kspar	Easting	Northing	Description
ML511		x	x	x	52 772036	7420578	Muscovite-bearing mylonite
ML512		x			52 700697	7434397	Muscovite-bearing mylonite zone with strong lineation, splay of Desert Bore Shear Zone
ML322		x			52 795705	7416246	Muscovite-bearing Heavitree Quartzite with muscovite lineation
ML323		x			52 777344	7430879	Garnet–muscovite–chlorite schist from mylonite zone
ML326	x				52 777344	7430879	Mafic amphibolite
ML327				x	52 761325	7428008	Hornblende–biotite migmatite with 1150 Ma metamorphic zircons
ML328	x		x		52 760833	7427781	Amphibolite from immediately south of mylonite sampled in ML329
ML329				x	52 760833	7427781	Muscovite-bearing sample from shear zone separating 1150 Ma migmatite from older gneisses
ML335		x			52 739475	7421879	Strained Heavitree Quartzite from shear zone
ML336				x	52 739475	7421879	Gneissic granite in basement below basement-cover unconformity
ML338		x			52 743120	7424400	Coarsely crystalline basement quartzite with abundant muscovite in main fabric
ML517		x			52 743120	7424400	Coarsely crystalline basement quartzite from Northern Range
ML520			x	x	52 743120	7424400	Felsic gneiss from basement interleaved with quartzite, from Northern Range
ML524				x	53 304100	7367900	Granitic clast from Areyonga Formation
ML525		x			52 634854	7430501	Muscovite-bearing mylonite from Mount Rennie

corresponding to the first released ^{39}Ar is used to give the activation energy, E_a, and the intercept, the frequency factor log (D_0/r_0^2). The factor r_0 is the reference length scale defined from the initial gas release to which all domains contribute. The computational routine used here calculates a distribution of activation energies (E_a), and uses a slab geometry to calculate the distribution of diffusion domain length scales (volume fraction and effective size). Each domain involves the same log D_0 and activation energy. As shown by Lovera *et al.* (1989) and Richter *et al.* (1991), a representation of the domain size distribution is given by the log(r/r_0) plot, in which the departure of the data from the linear array in the Arrhenius relationship is plotted against the volume fraction of ^{39}Ar released (Lovera *et al.*, 1991). The y-axis represents the size of the domains contributing ^{39}Ar at each stage in the experiment, relative to the reference length scale, r_0. The laboratory argon loss characteristics represented by the log(r/r_0) plot can be inverted to give the calculated domain size distribution in normalized form given that log(D_0) and the diffusion length scales cannot be known independently (McLaren *et al.*, 2007). As noted by Lovera *et al.* (2002), the calculated thermal history is largely independent of the chosen domain geometry, provided that the model parameters reproduce the observed laboratory argon loss and the laboratory age spectra and calculated log r/r_0 plots show a high-degree of cross-correlation. The calculated domain distribution is then inverted to yield temperature–time histories.

Here, this procedure was initially performed automatically, generating a series of 50 temperature-time paths (five different models for each of 10 calculated activation energies). A confidence interval about the calculated histories is then calculated, which gives modelled age spectra that are closest to those obtained during the laboratory step-heating experiment. The confidence intervals shown on the temperature–time paths (Fig. 6) indicate an uncertainty in model temperatures of around $\pm$ 25 °C, which is related mainly to the uncertainty in determining E_a. In cases where the automatic fitting of the age spectrum yields unsatisfactory results, or in cases where we have *a priori* geological constraints, we are also able to calculate temperature–time paths by inputting trial thermal histories and minimizing differences between the laboratory and modelled age spectra by iteration. We are able to model the laboratory age spectra using two end-member types of thermal histories: (1) continuous cooling and (2) thermal spikes associated with reheating. For the Mount Liebig samples, we initially discuss the results of modelling assuming continuous cooling histories. For the Ellery Creek sample we prefer a reheating scenario, as the sample analysed is from a boulder clast within the glacial Areyonga Formation. We then explore the implications of the best-fit reheating scenario for the Mount Liebig samples. The laboratory and best-fit model data are also presented in Fig. 7 in the form of Arrhenius and log r/r_0 plots, which allow comparison of the MDD solutions and the laboratory degassing data (Lovera *et al.*, 2002).

Mount Liebig region samples

K-feldspars ML336 and ML520 from the Mount Liebig region show a similar range of ages and similar best-fit thermal models. These two samples are from the central-western Mount Liebig area and are separated by an across strike distance of around 1.2 km including two major thrusts of the Amunurunga Thrust Complex (Scrimgeour *et al.*, 2005a). K-feldspar ML520, the most northerly of the pair, exhibits ages $\sim$40 Ma younger than K-feldspar ML336 throughout much of its age spectrum. Model fits for these samples suggest a two-stage cooling history (Fig. 6) with cooling episodes at 450 Ma and at around 330–280 Ma. These cooling episodes are separated by a period of apparently near isothermal residence. The maximum difference in modelled temperatures of these samples in this interval is 85 °C, with K-feldspar ML520, the most northerly sample, at higher temperature. This observation suggests thrusting from deeper levels in north during the interval 330–280 Ma. For an average thermal gradient of 30–35 °C km^{-1} in the overlying Amadeus Basin, movement must have been $<$2.5 km. Final closure of both samples occurred during the terminal ASO: For K-feldspar ML520 final closure to argon loss occurred around 325 Ma while K-feldspar ML336 recorded final closure around 280–300 Ma, implying southward structural younging in the Amunurunga Thrust Complex.

K-feldspars ML327, ML329 and ML511 were also modelled using the MDD method. Owing to the unusual form of these spectra, particularly over the first 40–60% gas released, we have chosen to perform coarse modelling only by fitting the modelled age spectra to the younger of all the contaminated steps (Fig. 6). The generally old ages indicate that these samples have not experienced temperatures in excess of 350 °C for any considerable time during the Palaeozoic or latest Neoproterozoic. For monotonic cooling histories, model fits for K-feldspar ML329 indicate a period of slow cooling between around 780 and 600 Ma followed by a period of isothermal residence. Final closure probably occurred during a period of rapid cooling around 330–300 Ma. K-feldspar ML327 suggests moderate cooling following the Teapot Orogenic Event at 1100–1200 Ma, and Palaeozoic cooling around 450–400 Ma. Final closure to argon loss probably occurred around 300 Ma. K-feldspar ML511 records a similar history of cooling at 1100 Ma with final cooling around 440 Ma.

Areyonga formation K-Feldspar

K-feldspar ML524 is from the Areyonga Formation Sturtian-aged diamictite conglomerate at Ellery Creek (Fig. 1). The sample shows a remarkably smooth monotonically rising age spectrum (Fig. 6) which suggests that it started to accumulate argon around 1100 Ma with final argon closure sometime in the Palaeozoic. Unfortunately, correction of the early released gas following the chlorine-related excess argon method of Harrison *et al.* (1994) was not successful owing to the low total production of ^{38}Ar.

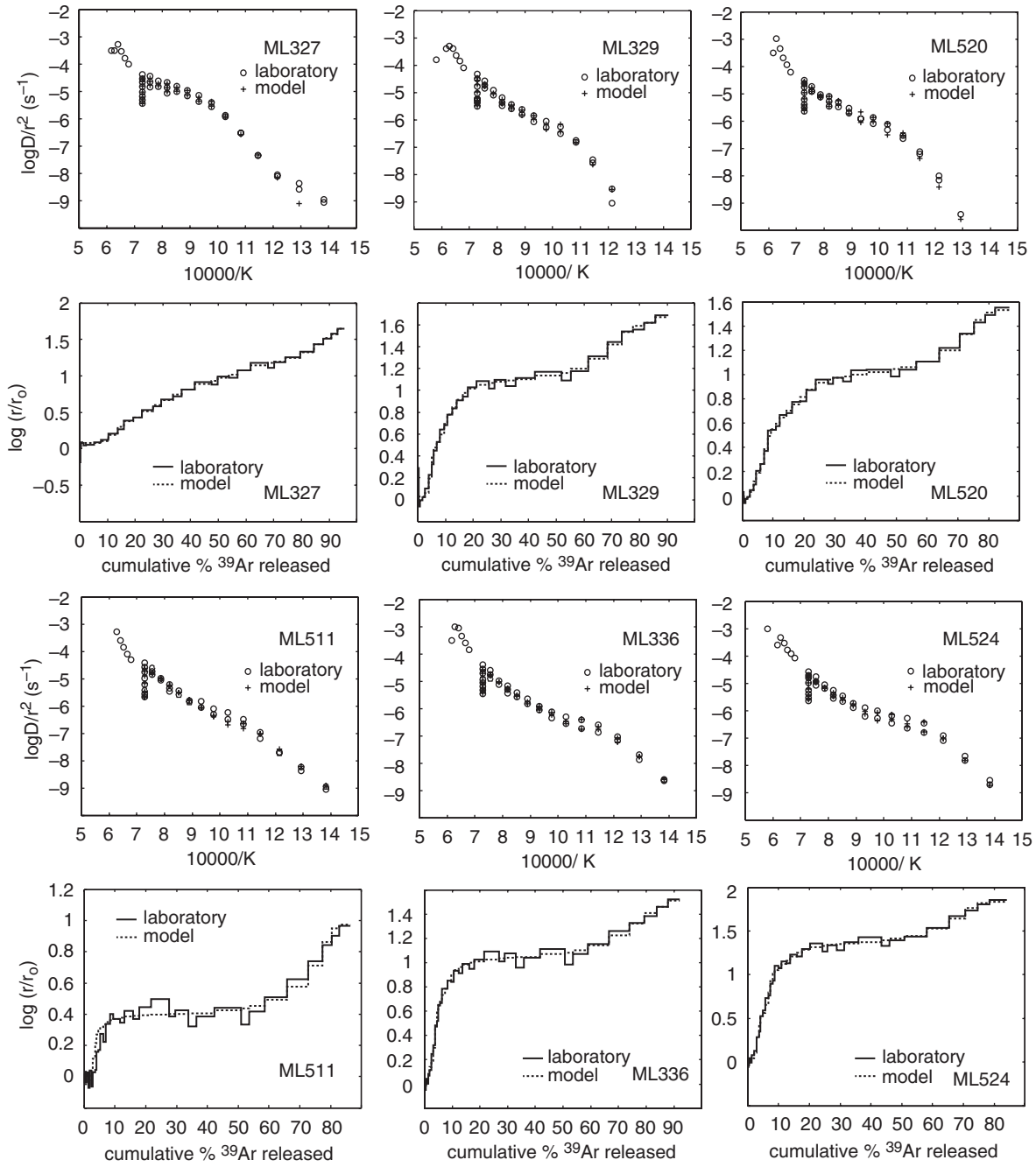

Fig. 7. Arrhenius and log r/r_o data for laboratory and model results for K-feldspar samples.

The relatively old ages are not surprising as the Ellery Creek sedimentary section is of very low metamorphic grade. Owing to the excess argon contained in the early released gas we are unable to robustly reconstruct the form of the reheating history, however, the ages recorded in this sample help to provide an upper limit on the maximum post-depositional temperatures recorded in the basin, and, thus, the maximum sediment thickness in the pre-orogenic Amadeus Basin.

Model fits suggest the sample cooled moderately slowly from 1100 Ma (following the Teapot Orogenic event) until at least 900 Ma, as indicated by the broad range of ages recorded in this interval. Around 900–800 Ma the sample must have cooled more rapidly, presumably as a result of a major exhumation event.

The Sturtian age of the conglomerate (*c*. 720–660 Ma; Lindsay, 1989; Corsetti *et al*., 2006) provides a key constraint on the cooling history. That is, the granitic boulder and its K-feldspar must have been at surface temperatures (*c*. 0 °C) at this time. The age spectrum is consistent with a period of slow reheating, at an average rate of ~0.5 °C/million years, that is in broad agreement with the known depositional history of the overlying sedimentary pile (e.g., Haines *et al*., 2001), suggesting there was no structural thickening of the basin before 400 Ma. Indeed, if K-feldspar ML524 had been reheated any more rapidly during

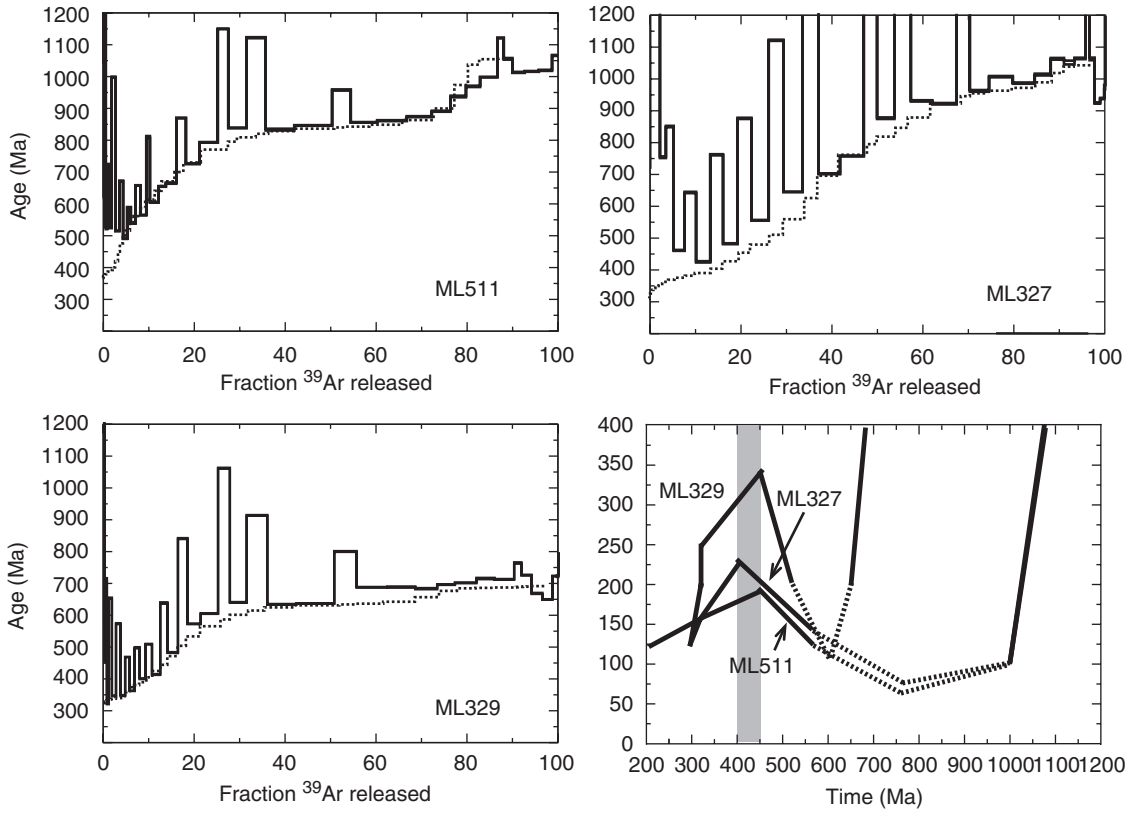

Fig. 8. Summary of reheating histories and best-fit thermal models for the Mount Liebig samples; *a priori* constraints consistent with the record of argon loss in K-feldspar ML524 from Ellery Creek have been used, as described in the text.

this interval, the record of slow cooling from 1100 Ma would have been erased. Moreover, the preservation of 800–1100 Ma cooling ages provides evidence that peak temperatures in the interval 780–400 Ma were *never* above 230 °C for extended periods of time, regardless of the heating rate, and were most likely to have been in the range 170–190 °C. These temperatures are consistent with the absence of evidence for new metamorphic mineral growth and, for a thermal gradient of 30–35 °C, imply that the sedimentary package overlying the Areyonga Formation before basin inversion was ~5–6 km thick. Chlorine-related excess argon contamination means that the timing of final closure to argon loss cannot be constrained precisely, however, the range of late Palaeozoic ages points to rapid cooling in the interval 400–330 Ma, coincident with main phase of compressional deformation during the ASO. This cooling resulted in final closure to argon loss.

Reheating histories

Section 'Mount Leibig region samples' described continuous cooling history models for the Mount Liebig samples recording a Proterozoic to Palaeozoic history. However, we are also able to explore model fits consistent with the style of reheating history implied by K-feldspar ML524 from Ellery Creek. Figure 8 shows the results of the best-fit models calculated with the *a priori* constraint of a thermal history in which reheating commences at around 800 Ma, coincident with burial beneath the evolving Centralian Superbasin. Maximum temperatures of reheating were unconstrained before modelling and determined only from the best-fit to the laboratory age spectra. These models show that each of the Mount Liebig K-feldspar samples are consistent with a reheating history, and in each case the oldest preserved cooling ages provide constraints on the maximum burial temperatures. Samples ML327 and ML511 are consistent with maximum temperatures of between 200 and 250 °C in the Palaeozoic (Fig. 8). The history of ML329 is somewhat different as this sample records a maximum age of only *c.* 700 Ma, suggesting much higher temperatures during the Palaeozoic. This is consistent with its location within a shear zone and implies shear zone reactivation during basin inversion.

For thermal gradients of ~30–35 °C km^{-1}, these modelled temperatures imply that samples ML327 and ML511 were exhumed from depths of around 6 to 8 km. As we are unable to precisely constrain the structural position of these samples with respect to the base of the basin, these depth estimates are likely to represent maximum estimates of the thickness of the overlying Centralian Superbasin before basin inversion. We do have good structural control on the position of K-feldspar ML336, however, as this sample was taken from a Warumpi Province gneissic granite immediately below the basement-cover unconformity (Fig. 2). The absence of ages greater than ~440 Ma in the age spectrum of K-feldspar ML336 implies that temperatures, at

least locally, exceeded *c*. 300–350 °C before, or during, Alice Springs aged deformation. In the absence of evidence for recrystallization, and for thermal gradients of around 30–35 °C/km, these temperatures suggest the possibility that the pre-orogenic Centralian Superbasin was as much as 8–10 km thick in the western Mount Liebig region.

DISCUSSION

The new data reported here extend the realm of Palaeozoic-aged deformation to the western Arunta and northwest Amadeus Basin and contribute to our understanding of the geometry of the Amadeus Basin before inversion during the ASO. The wide spread in apparent mineral ages of hornblende, muscovite and biotite recorded across the Mount Liebig region suggests that there has been partial argon loss in the interval from the latest Mesoproterozoic through until the late Palaeozoic and that reworking was spatially variable.

The generally old (1150–1840 Ma) ages recorded by the two hornblende samples analysed suggest that the highest-grade rocks experienced temperatures of around 500 °C before or around 1100 Ma during the Teapot Event. The absence of muscovite ages > 1000 to 1100 Ma suggests that many Warumpi Province shear zones were active before or during the Teapot Event and that temperatures throughout the region exceeded around 400 °C at this time.

Evolution of the Centralian Superbasin

Our new thermochronological data allow us to make inferences on aspects of the development and subsequent dismemberment of the Centralian Superbasin. First, the age spectra of muscovites ML338, ML511 and ML517 suggest that rocks of the Mount Liebig region cooled slowly from the Teapot Event until around 900–800 Ma. The exact nature of this second major cooling event around 800 Ma is enigmatic as there is no evidence for regional orogenic events yet recorded at this time. These *c*. 800 Ma cooling ages may reflect (1) cooling of the basement rocks due to movement on basement shear zones, implying that the initiation of the Centralian Superbasin was the result of active extension, or (2) long-term slow cooling due to gravitational re-equilibration following orogeny, as reported for the Norwegian Grenville Provinces (Willigers *et al*., 2002) and the Halls Creek Orogen (Bodorkos & Reddy, 2004).

Second, the range of ages recorded by age spectra of K-feldspars provides constraints on the maximum thickness of the Centralian Superbasin sediments. For thermal gradients of ~30 to 35 °C km^{-1}, consistent with measured modern day thermal gradients as well as the presence of high heat producing basement rocks beneath the evolving Amadeus Basin (e.g., Sandiford, 2002), the K-feldspar $^{40}Ar/^{39}Ar$ data from the Areyonga Formation at Ellery Creek imply the presence of around 5–6 km of overlying sediment before Palaeozoic unroofing. This is consistent with vitrinite maturation (Jackson *et al*., 1984) and apatite fission track data (Tingate, 1991), and, when the thickness of underlying Succession 1 sediments is taken into account, points to a total thickness of the Amadeus Basin before the ASO of > 7 km. Basement K-feldspars imply higher temperatures (around 250–350 °C) in the interval from the late Neoproterozoic to the Ordovician suggesting exhumation, and therefore the thickness of the Centralian Superbasin sediments, was greater over the Arunta Region basement. Moreover, results found for the two most northerly basement K-feldspars (ML327 and ML329) are consistent with higher temperatures in this interval, an observation that is consistent with, though not necessarily unequivocal support for, the suggestion of northward deepening of the Centralian Superbasin. More thermochronological data from further north within the Arunta Region, taken from samples on which we have good structural control, are required to rigorously test whether or not the Centralian Superbasin was continuous across the now exhumed basement blocks.

Palaeozoic reworking and the ASO

Cooling ages of 520–480 Ma recorded by Muscovite ML512, from a splay of the Desert Bore Shear Zone in the Tjungkuba Hills, are the oldest Palaeozoic ages recorded in the western Arunta Region. These ages may reflect slow cooling related to exhumation during the 570–530 Ma Petermann Ranges Orogeny. Thin section examination of the sample reveals a composite texture and the presence of two populations of muscovite – coarse platy fish-like muscovite grains, and finer aggregates of recrystallized muscovite. As the fish-like grains are much coarser, the majority of the mineral separate analysed probably consists of these grains. This is supported by the form of the age spectrum, which does not exhibit any of the characteristics of a mixed population. Accepting this, the age spectrum of this sample suggests that the sample may have closed slowly in the period between 520 and 480 Ma. The youngest ages around 460–440 may reflect resetting at this time, possibly due to recrystallization of the finer muscovite fraction during the earliest compressional ASO. If the *c*. 500 Ma ages reflect cooling of pre-existing grains, this observation provides evidence that the Desert Bore Shear Zone is a long-lived feature and that at least some movement on the structure predates the ASO.

Evidence for subsequent Palaeozoic reworking is recorded by muscovite, biotite and K-feldspar thermochronometers. Importantly, the range of recorded muscovite ages between 440 and 300 Ma (Fig. 4) points to thermal disturbance from the Silurian through until the late Carboniferous and suggests final cooling and exhumation of the terrane in this interval. Moreover, neoformed fine-grained muscovite from mylonite zones with plateau-like ages of around 375 Ma (sample ML335) and around 400 Ma (sample ML323) suggests that new mineral growth dates from the earliest ASO and was restricted to

shear zones, many of which appear to be reactivated Proterozoic structures (e.g., Shaw & Black, 1991). Importantly there is no evidence in the Mount Liebig region for active deformation and/or new mineral growth in the late stages of the ASO in the interval 350–300 Ma.

Together these data suggest that Palaeozoic deformation in the Mount Liebig area began during the earliest compressional stages of the ASO, in the period 440–380 Ma, with ongoing cooling extending throughout the ASO until the late Carboniferous. Although these ages define an orogenic episode of ~140 million years duration, assigning all mid-Ordovician and Devonian tectonism to the ASO is consistent with the original definition of the event (Forman *et al.*, 1967; Bradshaw & Evans, 1988) as well as more recent work (e.g., Haines *et al.*, 2001; Maidment *et al.*, 2007). The range of apparent deformation and/or cooling ages recorded within this interval (see compilation in Haines *et al.*, 2001) suggests that the ASO *sensu lato* was diachronous. The oldest ages of *c.* 440–380 Ma from Mount Liebig are consistent with the generally older ages (*c.* 440–380 Ma) recorded in the Strangways Range, north of the Ngalia Basin (Möller *et al.*, 1999; Ballèvre *et al.*, 2000) and the North East Arunta (Buick *et al.*, 2001; Scrimgeour & Raith, 2001). This, together with the absence of younger deformation ages, suggests the ASO-aged deformation ceased early in the Mount Liebig area; consistent with a shift from a major E–W trending thick-skinned orogen in the early ASO to a more areally restricted, higher geothermal gradient event during the late ASO (350–300 Ma; Dunlap & Teyssier, 1995; Hand *et al.*, 1999; Mawby *et al.*, 1999). The data from the Mount Liebig region are also broadly consistent with $^{40}Ar/^{39}Ar$ data from mylonites in the vicinity of the Redbank Shear Zone (Biermeier *et al.*, 2003) where hornblende typically preserves cooling ages from the Teapot Event (*c.* 1150 Ma), and biotite recrystallized in mylonite zones records older ASO ages in the range 450–400 Ma.

Models for intraplate orogenesis

As noted in the Introduction, debate on the factors controlling inversion of the Centralian Superbasin during the Petermann Ranges and Alice Springs Orogenies has centred largely on the role of inherited structures (e.g., Braun & Shaw, 2001; Camacho *et al.*, 2002) and the impact of thermal weakening due to the presence of high-heat-producing basement rocks beneath the basin (e.g., Hand & Sandiford, 1999; Sandiford *et al.*, 2001). Criticism of the 'thermal blanket' model is based on the preservation of Mesoproterozoic muscovite argon ages in the Musgrave Region basement, as well as the population of apparently Musgrave Region-aged detrital zircons (in the range 1.2–1.05 Ga) reported from pre- and syn-orogenic sediments of Neoproterozoic to early Cambrian age in the southern Amadeus Basin by Camacho *et al.* (2002). However, as shown more recently by Maidment *et al.* (2007), a similar Grenvillian-aged (*c.* 1.2–1.0 Ga) detrital zircon population occurring in late Cambrian and Ordovician sediments in the Amadeus Basin may be attributed to a component of distal 'Pacific Gondwanan' sources. Moreover, improved characterization of the range of ages of both granites and metasediments in the Musgrave Region gives, in terms of decreasing abundance, populations of igneous zircons around 1.16–1.22, 1.307–1.34 and 1.065–1.08 Ga, as well as a spread of Mesoproterozoic to Palaeoproterozoic metasedimentary zircons between 1.32 and 1.79 Ga in age (H. Smithies, pers. comm., 2008). Sediments sourced from the Musgrave Region should show zircon distributions equivalent to these populations. Together these observations raise the possibility that the detrital zircon populations identified by Camacho *et al.* (2002) in the pre- and syn-orogenic sediments of the southern Amadeus Basin could reflect distal, rather than local Musgrave Region sources.

Nonetheless, even if the detrital zircon populations reported from Neoproterozoic to early Cambrian sediments in the southern Amadeus Basin do reflect sourcing from the Musgrave region, therefore casting doubt on the 'thermal blanket' model for the Petermann Ranges Orogeny, the new data reported here provide a compelling case that radiogenic heating in response to burial was responsible for the onset of the ASO in the northern Amadeus Basin. The suggestion that sediment thickness increased to the north over the now exposed southern margin of the Arunta Region supports the suggestion of Sandiford & Hand (1998) that deformation was focused in areas of thickest sedimentary cover. Moreover, the record of reheating in the Neoproterozoic to early Palaeozoic suggests that there was no dramatic thickening of the sedimentary pile before deformation and that basin inversion occurred in response to burial at rates consistent with deposition of the Amadeus Basin sedimentary package.

Importantly, our results are also consistent with the pattern of detrital zircon data reported for sediments of the Amadeus and Georgina Basins by Maidment *et al.* (2007) and others. As shown in Fig. 3, these previously reported detrital zircon populations show: (1) Arunta-aged zircons within the Neoproterozoic sediments of Successions 1 and 2 and Ediacaran-aged sediments of Succession 3; (2) a general absence of Grenvillian-aged zircons in Succession 3 sediments immediately before the Petermann Ranges Orogeny; and (3) the general absence of Arunta-aged zircons within both Cambrian–Ordovician and Silurian–Devonian sediments of the Amadeus and Georgina Basins, a period of more than 100 million years leading up to the ASO. Together with our thermochronological data, these results provide evidence for a thick sedimentary pile over the now exposed southern Arunta Region. It is likely that at least some Arunta-aged basement, probably in the northwest, may have remained emergent during the early evolution of the Centralian Superbasin and that over time the basin extended northward and more of the basement was buried beneath the sedimentary pile. This conclusion is consistent with the Centralian Superbasin geometry originally proposed by Walter *et al.* (1995).

ACKNOWLEDGEMENTS

We are grateful to the people of the Papunya, Haasts Bluff and Mount Liebig communities and to the Central Land Council for access to the Mount Liebig area. We thank John Mya, Shane Paxton, Robyn Maier and Xiaodong Zhang for technical assistance. Irradiations were undertaken by the Australian Nuclear Science and Technology Organization, through the Australian Institute of Nuclear Science and Engineering. We thank Russell Korsch, Peter van der Beek and two anonymous reviewers for their detailed reviews of the manuscript. SM acknowledges ARC Discovery Grant DP0208837 for support during analysis and a University of Melbourne Centenary Research Fellowship for support during publication.

REFERENCES

Ballèvre, M., Moller, A. & Henson, B. (2000) Exhumation of the lower crust during crustal shortening: an Alice Springs (380 Ma) age for a prograde amphibolite-facies shear zone in the Strangways Metamorphic Complex (central Australia). *J. Metamorph. Geol.*, **18**, 737–747.

Biermeier, C., Stüwe, K., Foster, D.A. & Finger, F. (2003) Thermal evolution of the Redbank thrust system, central Australia: geochronological and phase-equilibrium constraints. *Tectonics*, **22**, doi: 10.1029/2001TC901033.

Bodorkos, S. & Reddy, S.M. (2004) Proterozoic cooling and exhumation of the northern central Halls Creek Orogen, Western Australia: constraints from a reconnaissance $^{40}Ar/^{39}Ar$ study. *Aust. J. Earth Sci.*, **51**, 591–609.

Bradshaw, J.D. & Evans, P.R. (1988) Palaeozoic tectonics, Amadeus Basin, central Australia. *Aust. Petrol. Explorat. Assoc. J.*, **28**, 267–282.

Braun, J. & Shaw, R. (2001) A thin-plate model of Palaeozoic deformation of the Australian lithosphere: implications for understanding the dynamics of intracratonic deformation. *Geol. Soc. Lond. Spec. Publ.*, **184**, 165–193.

Buick, I.S., Miller, J.A., Williams, I.S. & Cartwright, I. (2001) Ordovician high-grade metamorphism of a newly recognised late Neoproterozoic terrane in the northern Harts Range, central Australia. *J. Metamorph. Geol.*, **19**, 373–394.

Camacho, A., Compston, W., McCulloch, M. & McDougall, I. (1997) Timing and exhumation of eclogite facies shear zones, Musgrave Block, central Australia. *J. Metamorph. Geol.*, **15**, 735–751.

Camacho, A., Hensen, B.J. & Armstrong, R. (2002) Isotopic test of a thermally driven intraplate orogenic model, Australia. *Geology*, **30**, 887–890, doi: 10.1130/0091-7613.

Collins, W.J. & Teyssier, C. (1989) Crustal scale ductile fault systems in the Arunta Inlier, central Australia. *Tectonophysics*, **158**, 49–66.

Corsetti, F.A., Stewart, J.H. & Hagadorn, J.W. (2006) Neoproterozoic diamictite-cap carbonate succession and $\partial^{13}C$ chemostratigraphy from Eastern Sonora, Mexico. *Chem. Geol.*, **237**, 129–142.

Dahl, P.S. (1996) The crystal-chemical basis for Ar retention in micas: inferences from interlayer partitioning and implications for geochronology. *Contrib. Mineral. Petrol.*, **123**, 22–39.

Dunlap, W.J. (2000) Natures diffusion experiment; the cooling-rate cooling-age correlation. *Geology*, **28**, 139–142.

Dunlap, W.J., Hirth, G. & Teyssier, C. (1997) Thermomechanical evolution of a ductile duplex. *Tectonics*, **16**, 983–1000.

Dunlap, W.J. & Teyssier, C. (1995) Palaeozoic deformation and isotopic disturbance in the southeastern Arunta Block, central Australia. *Precamb. Res.*, **71**, 229–250.

Edgoose, C.J., Scrimgeour, I.R. & Close, D.F. (2004) Geology of the Musgrave Block, Northern Territory. Northern Territory Geological Survey Report.

Flöttmann, T. & Hand, M. (1999) Folded basement-cores tectonic wedges along the northern edge of the Amadeus basin, central Australia: evaluation of orogenic shortening. *J. Struct. Geol.*, **21**, 399–412.

Forman, D.J. (1966) The geology of the south-western margin of the Amadeus Basin, Central Australia. Bureau of Mineral Resources Report 87.

Forman, D.J., Milligan, E.N. & McCarthy, W.R. (1967) Regional geology and structure of the northeast margin of the Amadeus Basin, Northern Territory. Bureau of Mineral Resources Report 103.

Gorter, J.D. (1984) Source potential of the Horn Valley siltstone, Amadeus Basin. *Aust. Petrol. Explorat. Assoc. J.*, **24**, 66–90.

Haines, P.W., Hand, M. & Sandiford, M. (2001) Palaeozoic synorogenic sedimentation in central and northern Australia: a review of distribution and timing with implications for the evolution of intracontinental orogens. *Aust. J. Earth Sci.*, **48**, 911–928.

Hames, W.E. & Bowring, S.A. (1994) An empirical evaluation of the argon diffusion geometry in muscovite. *Earth Planet. Sci. Lett.*, **124**, 161–169.

Hames, W.E. & Cheney, J.T. (1997) On the loss of $^{40}Ar^*$ from muscovite during polymetamorphism. *Geochim. Cosmochim. Acta*, **61**, 3863–3872.

Hand, M., Mawby, J., Kinny, P. & Foden, J. (1999) U-Pb ages from the Harts Range, central Australia: evidence for early Ordovician extension and constraints on Carboniferous metamorphism. *J. Geol. Soc.*, **156**, 715–730.

Hand, M. & Sandiford, M. (1999) Intraplate deformation in central Australia: the link between subsidence and fault reactivation. *Tectonophysics*, **305**, 121–140.

Harrison, T.M. (1981) Diffusion of ^{40}Ar in hornblende. *Contributions to Mineralogy and Petrology*, **78**, 324–331.

Harrison, T.M., Duncan, I. & McDougall, I. (1985) Diffusion of ^{40}Ar in biotite: temperature, pressure and compositional effects. *Geochim. Cosmochim. Acta*, **49**, 2461–2468.

Harrison, T.M., Heizler, M.T., Lovera, O.M., Chen, W. & Grove, M. (1994) A chlorine-disinfectant for excess argon released from K-feldspar during step-heating. *Earth Planet. Sci. Lett.*, **123**, 95–104.

Jackson, K.S., McKirdy, D.M. & Deckelman, J.A. (1984) Hydrocarbon generation in the Amadeus Basin. *Aust. Petrol. Explorat. Assoc. (APEA) J.*, **24**, 42–65.

Kinny, P.D. (2002) SHRIMP U-Pb geochronology of Arunta Province samples from the Mount Liebig and lake Mackay 1:250 000 mapsheets. Northern Territory Geological Survey, Technical Note, 2002-015.

Korsch, R.J. & Lindsay, J.F. (1989) Relationships between deformation and basin evolution in the intracratonic Amadeus Basin, Central Australia. In: *Deformation of Crustal Rocks* (Ed. by A. Ord), Tectonophysics **158**, 5–22.

Lindsay, J.F. (1989) Depositional controls on glacial facies associations in a basinal setting, late Proterozoic, Amadeus Basin, central Australia. *Palaeogeogr. Palaeoclimatol., Palaeoecol.*, **73**, 205–232.

Lindsay, J.F. & Korsch, R.J. (1991) The evolution of the Amadeus Basin, central Australia. *Bureau Miner. Resources Aust. Bull.*, **236**, 7–32.

Lo, C-H., Lee, J.K.W. & Onstott, T.C. (2000) Argon release mechanisms of biotite in vacuo and the role of short-circuit diffusion and recoil. *Chem. Geol.*, **165**, 135–166.

Lovera, O.M., Grove, M. & Harrison, T.M. (2002) Systematic analysis of K-feldspar $^{40}Ar/^{39}Ar$ step heating results II: relevance of laboratory argon diffusion properties to nature. *Geochim. Cosmochim. Acta*, **66**(7), 1237–1255.

Lovera, O.M., Richter, F.M. & Harrison, T.M. (1989) The $^{40}Ar/^{39}Ar$ thermochronometry for slowly cooled samples having a distribution of diffusion domain sizes. *J. Geophys. Res.*, **94**, 17917–17935.

Lovera, O.M., Richter, F.M. & Harrison, T.M. (1991) Diffusion domains determined by AR-39 released during step heating. *J. Geophys. Res.*, **96**, 2057–2069.

Maidment, D.W., Williams, I.S. & Hand, M. (2007) Testing long-term patterns of basin sedimentation by detrital zircon geochronology, Centralian Superbasin, Australia. *Basin Res.*, **19**, 335–360.

Marjoribanks, R.W. (1976) Basement and cover relations on the northern margin of the Amadeus Basin, central Australia. *Tectonophysics*, **33**, 15–32.

Mathur, S.P. (1976) Relation of Bouguer anaomalies to crustal structure in southwestern and central Australia. *Bureau Mineral Resources J. Aust. Geol. Geophys.*, **1**, 277–286.

Mawby, J., Hand, M. & Foden, J. (1999) Sm-Nd evidence for high-grade Ordovician metamorphism in the Arunta Block, central Australia. *J. Metamorph. Geol.*, **17**, 653–668.

McDougall, I. & Harrison, T.M. (1999) *Geochronology and Thermochronology by the $^{40}Ar/^{39}Ar$ Method*, 2nd ed, 269pp. Oxford University Press, New York.

McDougall, I. & Roksandic, Z. (1974) Total fusion $^{40}Ar/^{39}Ar$ ages using HIFAR reactor. *J. Geol. Soc. Aust.*, **21**, 81–89.

McLaren, S. & Dunlap, W.J. (2006) The use of $^{40}Ar/^{39}Ar$ K-feldspar thermochronology in basin thermal history reconstruction: an example from the Big Lake Suite granites, Warburton Basin, South Australia. *Basin Res.*, **18**, 189–203, doi: 10.1111/j.1365-2117.2006.00288.x.

McLaren, S., Dunlap, W.J. & Powell, R. (2007) Understanding K-feldspar $^{40}Ar/^{39}Ar$ data: reconciling models, methods and microtextures. *J. Geol. Soc.*, **164**, 941–944.

McLaren, S., Dunlap, W.J., Sandiford, M. & McDougall, I. (2002) Thermochronology of high heat producing crust at Mount Painter, South Australia: implications for tectonic reactivation of continental interiors. *Tectonics*, **21**, 4, doi: 10.1029/2000TC001275.

Möller, A., Williams, I.S., Jackson, S. & Henson, B.S. (1999) Palaeozoic deformation and mineral growth in the Strangways Metamorphic Complex: *in-situ* dating of zircon and monazite in a staurolite-corundum bearing shear zone. *Geol. Soc. Aust. Abstracts*, **54**, 71.

Page, R. (1996) Sample 2000082005. Unpublished data in Geoscience Australia OZCHRON geochronology database. http://www.ga.gov.au.

Parsons, I., Brown, W.L. & Smith, J.V. (1999) $^{40}Ar/^{39}Ar$ thermochronology using alkali feldspars: real thermal history or mathematical mirage of microtexture? *Contrib. Mineral. Petrol.*, **136**, 92–110.

Renne, P.R., Swisher, C.C., Deino, A.L., Karner, D.B., Owens, T.L. & DePaolo, D.J. (1998) Intercalibration of standards, absolute ages and uncertainties in $^{40}Ar/^{39}Ar$ dating. *Chem. Geol.*, **145**, 117–152.

Richter, F.M., Lovera, O.M., Harrison, T.M. & Copeland, P. (1991) Tibetan tectonics from $^{40}Ar/^{39}Ar$ analysis of a single K-feldspar sample. *Earth Planet. Sci. Lett.*, **105**, 266–278.

Sandiford, M. (2002) Low thermal peclet number intraplate orogeny in central Australia. *Earth Planet. Sci. Lett.*, **201**, 309–320.

Sandiford, M. & Hand, M. (1998) Controls on the locus of intraplate deformation in central Australia. *Earth Planet. Sci. Lett.*, **162**, 97–110.

Sandiford, M., Hand, M. & McLaren, S. (2001) Tectonic feedback, intraplate orogeny and the geochemical structure of the crust: a central Australian perspective. In: *Continental Reactivation and Reworking* ((Ed. by J. Miller, R. Holdsworth, I. Buick & M. Hand), *Geol. Soc. Spec. Publ.*, 184, 195–218.

Scaillet, S., Fjbaud, G., Ballevre, M. & Amouric, M. (1992) Mg/Fe and [(Mg, Fe) Si-Al_2] compositional control on argon behaviour in high-pressure white micas: a $^{40}Ar/^{39}Ar$ continuous laser-probe study from the Dora-Maira nappe of the internal western Alps, Italy. *Geochim. Cosmochim. Acta*, **56**, 2851–2872.

Scrimgeour, I. & Raith, J.G. (2001) Tectonic and thermal events in the northeastern Arunta Province. Northern Territory Geological Survey, Report 12, 45pp.

Scrimgeour, I.R. & Close, D.F. (1999) Regional high-pressure metamorphism during intracratonic deformation: the Petermann Orogeny, central Australia. *J. Metamorph. Geol.*, **17**, 557–572.

Scrimgeour, I.R., Close, D.F. & Edgoose, C.J. (2005a) *Explanatory Notes, 1:250 000 Geological Map Series, Mount Liebig SF52-16*, 2nd edn. Northern Territory Geological Survey, Darwin.

Scrimgeour, I.R., Kinny, P.D., Close, D.F. & Edgoose, C.J. (2005b) High-T granulites and polymetamorphism in the southern Arunta Region, central Australia: evidence for a 1.64 Ga accretional event. *Precambr. Res.*, **142**, 1–27.

Shaw, R.D. (1991) The tectonic development of the Amadeus Basin, central Australia. *Bureau Miner. Resources Aust. Bull.*, **236**, 429–461.

Shaw, R.D. & Black, L.P. (1991) The history and tectonic implications of the Redbank Thrust Zone, central Australia, based on structural, metamorphic and Rb-Sr isotopic evidence. *Aust. J. Earth Sci.*, **38**, 307–332.

Shaw, R.D., Zeitler, P.K., McDougall, I. & Tingate, P.R. (1992) The Palaeozoic history of an unusual intracratonic thrust belt in central Australia based on $^{40}Ar/^{39}Ar$, K-Ar and fission track dating. *J. Geol. Soc. Lond.*, **149**, 937–954.

Steiger, R. & Jäger, E. (1977) Subcommission on geochronology: convention on the use of decay constants in geo- and cosmochronology. *Earth Planet. Sci. Lett.*, **36**, 359–362.

Tetley, N., McDougall, I. & Heydegger, H.R. (1980) Thermal neutron interferences in the $^{40}Ar/^{39}Ar$ dating technique. *J. Geophys. Res.*, **85**, 7201–7205.

Teyssier, C. (1985) A crustal thrust system in an intracratonic tectonic environment. *J. Struct. Geol.*, **7**, 689–700.

Teyssier, C., Amri, C. & Hobbs, B.E. (1988) South Arunta Block: the internal zones of a Proterozoic overthrust in central Australia. *Precambr. Res.*, **40/41**, 157–173.

Tingate, P.R. (1991) Apatite fission track analysis of the Pacoota and Stairway Sandstones, Amadeus Basin, central Australia. *Bureau Miner. Resources Aust. Bull.*, **236**, 525–540.

Walter, M.R., Veevers, J.J., Calver, C.R. & Grey, K. (1995) Neoproterozoic stratigraphy of the Centralian Superbasin. *Precambr. Res.*, **73**, 173–195.

Wells, A.T. (1981) Late Proterozoic diamictites of the Amadeus and Ngalia Basins, central Australia. In: *Earth's pre-Pleistocene glacial record (Cambridge Earth Sciences Series)* (Ed. by M.J. Hambrey & W.B. Harland) Cambridge University Press, Cambridge, pp. 515–524.

Willigers, B.J.A., van Gool, J.A.M., Wijbrans, J.R., Krogstad, E.J. & Mezger, K. (2002) Post tectonic cooling of the Nagssugtoqidian Orogen and a comparison of contrasting cooling histories in Precambrian and Phanerozoic Orogens. *J. Geol.*, **110**, 503–517.

Zhao, J.-X., McCulloch, M.T. & Bennett, V.C. (1992) Sm-Nd and U-Pb zircon isotopic constraints on the provenance of sediments from the Amadeus Basin, central Australia: evidence for REE fractionation. *Geochim. Cosmochim. Acta*, **56**, 921–940.

Manuscript received 21 February 2008; Manuscript accepted 27 August 2008.

APPENDIX $^{40}Ar/^{39}Ar$ ANALYTICAL PROCEDURE

Mineral separation was carried out using routine heavy liquid flotation, and magnetic methods. In addition, muscovite from samples ML322, ML323 and ML335 was concentrated using heavy liquid centrifuge techniques. All samples were concentrated to better than 99%, with the principal impurities being mineral and fluid inclusions. Most K-feldspars were sized between 125 and 350 μm using standard mesh sieves. Most micas were sized between 90 and 250 μm; muscovite ML322, ML323 and ML335 were sized <75 μm. Hornblendes were sized between 100 and 250 μm.

Samples were irradiated for 480 h in facilities X33 or X34 of the Australian Nuclear Science and Technology Organization HIFAR reactor, Lucas Heights, NSW. Samples were packed in aluminium cans with a number of splits of the fluence monitor biotite GA1550 (with K/Ar age, 98.79 Ma, McDougall & Roksandic, 1974; Renne *et al.*, 1998). The sample can was inverted 180° three times during the irradiation to minimize the effect of the large neutron flux gradient along the length of the can. A cadmium liner was used to minimize interference from thermal neutrons. Irradiation time was chosen in order to achieve a $^{40}Ar^*/^{39}Ar_K$ ratio of $\sim$20.

$^{40}Ar/^{39}Ar$ analysis was undertaken at the Research School of Earth Sciences at the Australian National University. During step-heating experiments the temperature was monitored using a thermocouple at the base of a tantalum crucible within a double-vacuum resistance furnace. Temperatures were progressively increased over the course of the gas extraction, with temperatures and times of each step chosen to give an even gas release. The heating schedule for hornblende samples commenced at 900–1400 °C; biotite from 600 °C to 1350 °C; muscovite from 530 °C to 750 °C (depending on grain size) to 1350 °C, and

Table 2. Calculated domain distributions for K-feldspar samples

Domain	Log D_0 cm^2 s^{-1}	Volume fraction (%) ϕ_j	Domain size (Relative) ρ_j
K-feldspar ML327, $E_a = 55 \pm 2$ kcal mol^{-1}			
1	8.22415	8.108	0.00049
2	7.14532	8.391	0.00170
3	6.37921	9.279	0.00411
4	5.44660	17.421	0.01203
5	4.53278	12.197	0.03446
6	4.53227	22.062	0.03448
7	3.66764	19.103	0.09330
8	1.60740	3.438	1.00000
K-feldspar ML329, $E_a = 59 \pm 4$ kcal mol^{-1}			
1	9.92309	3.687	0.00072
2	8.42909	2.943	0.00405
3	7.59021	2.972	0.01063
4	5.45376	33.767	0.12435
5	5.45370	17.307	0.12436
6	4.41113	21.961	0.41302
7	3.90912	6.420	0.73618
8	3.64308	10.943	1.00000
K-feldspar ML336, $E_a = 43 \pm 3$ kcal mol^{-1}			
1	8.26922	0.543	0.00024
2	7.01891	2.666	0.00099
3	5.32567	2.216	0.00697
4	2.68998	38.015	0.14490
5	2.66828	16.400	0.14856
6	2.16960	6.522	0.26379
7	1.76006	23.980	0.42269
8	1.01210	9.659	1.00000
K-feldspar ML511, $E_a = 37 \pm 2$ kcal mol^{-1}			
1	5.23964	2.032	0.00246
2	1.56195	4.077	0.16994
3	1.55734	17.529	0.17084
4	1.55621	14.729	0.17106
5	1.55588	13.654	0.17113
6	1.54672	17.731	0.17294
7	0.20482	22.814	0.81069
8	0.02253	7.434	1.00000
K-feldspar ML520, $E_a = 57 \pm 4$ kcal mol^{-1}			
1	8.64143	1.781	0.00099
2	7.64027	3.732	0.00314
3	6.45916	2.111	0.01224
4	5.77676	3.902	0.02685
5	5.77345	1.583	0.02695
6	3.99407	49.362	0.20908
7	3.52345	3.723	0.35944
8	2.63470	33.806	1.00000
K-feldspar ML524, $E_a = 47 \pm 3$ kcal mol^{-1}			
1	8.44899	2.572	0.00052
2	6.86681	3.268	0.00324
3	5.10552	2.858	0.02463
4	3.19105	24.706	0.22323
5	3.18059	13.885	0.22593
6	3.10682	8.926	0.24596
7	3.09997	2.628	0.24791
8	1.88854	41.157	1.00000

K-feldspar samples were subject to a series of 43 steps at temperatures between 450 °C and 1450 °C (including many duplicate or triplicate isothermal steps). The schedule of heating times and temperatures for each sample can be found in Table 1 (hornblende, muscovite and biotite samples), and Table 2 (K-feldspar samples).

After each temperature step, the gas released was exposed to Zr–Al getters to remove all active gases; gettering time in the vacuum line was generally ~10 min. Subsequently the purified argon was analysed in the mass spectrometer. For most samples isotopic analysis was performed using a VG Isotech MM3600 gas source mass spectrometer, operated in the static mode. Measurement was made using a Daly collector and photomultiplier with overall sensitivity $\sim 4.0 \times 10^{-17}$ mol mV^{-1}. For samples ML338 (muscovite), ML328 (biotite), ML328 (hornblende) and ML326 (hornblende) isotopic analysis was performed using a VG Isotech MM1200 gas source mass spectrometer, also operated in the static mode. Ion beam measurements were made using an electron multiplier with sensitivity of $\sim 8.0 \times 10^{-15}$ mol mV^{-1}. Corrections for argon produced by interactions of neutrons with K and Ca were made (Tetley *et al.*, 1980). The ^{40}K abundance and decay constants employed were those recommended by the IUGS Subcommission on Geochronology (Steiger & Jäger, 1977).